Comment on “Perturbation theory of scattering for grazing-incidence fast-atom diffraction”, by W. Allison, S. Miret-Artés and E. Pollak, Phys. Chem. Chem. Phys. , 2022, 24 , 15851

Gisela Anahí Bocan, Hanadi Breiss, Samir Szilasi, Anouchah Momeni, Esteban Alejandro Sánchez, María Silvia Gravielle, Hocine Khemliche, E.M. Staicu Casagrande

PCCP

ARTICLE TYPE

Cite this: DOI: 00.0000/xxxxxxxxxx

Comment on "Perturbation theory of scattering for grazing-incidence fast-atom diffraction", by W. Allison, S. Miret-Artés and E. Pollak, PCCP 2022, 24, 15851

Gisela Anahí Bocan,[*,a] Hanadi Breiss,[b] Samir Szilasi,[b] Anouchah Momeni,[b,c] Elena Magdalena Staicu Casagrande,[b] Esteban Alejandro Sánchez,[a,d] María Silvia Gravielle,[*,e] and Hocine Khemliche[b]

Received Date
Accepted Date

DOI: 00.0000/xxxxxxxxxx

In this comment we discuss some aspects of Phys. Chem. Chem. Phys. 2022, **24**, 15851, by Allison *et al.*, an article intensely motivated by our study of grazing incidence fast atom diffraction (GIFAD) for He-KCl(001) [Phys. Rev. Lett. 2020, **125**, 096101; Phys. Rev. B. 2021, **104**, 235401]. In particular, a) we show that, contrary to first order perturbation prediction, the surface corrugation is not proportional to the tangent of the rainbow angle and, b) we analyze whether a Morse-like formula, like the one Allison *et al.* use, is able to reproduce the atom-surface potential derived from density functional theory (DFT) calculations. In addition, we give some clarifications regarding specific remarks the authors made about our articles.

1 Introduction

Grazing Incidence Fast Atom Diffraction (GIFAD) has recently emerged as a powerful surface analysis technique [1]. Its grazing geometry makes it suitable for in-situ monitoring of thin film growth, and thus an appealing alternative to reflection high energy electron diffraction (RHEED), given it is less invasive, more surface sensitive and readily interpretable quantitatively [2].

In recent publications [3,4], we analyzed the behavior of the surface corrugation and the rainbow angle, two GIFAD related quantities, for very low normal energy ($E_\perp$) He atoms impinging on a KCl(001) surface. Some aspects of our study have been commented on in the article Phys. Chem. Chem. Phys. 2022, **24**, 15851 by Allison *et al* [5]. In their argumentation the authors have assumed the applicability of classical first order perturbation (FOP) theory to this problem, and obtained the rainbow angle dependence on the normal energy that results from modeling the axial interaction potential with a Morse-like function.

In this comment we will show that very low $E_\perp$ GIFAD for He-KCl(001) cannot be properly described in terms of classical FOP theory and that a realistic potential for this system and scattering process cannot be satisfactorily fitted with the proposed Morse-like formula. This paper is organized as follows: In Sec. 2 we analyze the applicability of FPO to low-$E_\perp$ GIFAD for He-KCl(001); in Sec. 3, we compare our DFT potential with a Morse-like one; in Secs. 4 and 5 we respond to some specific claims the authors made about our articles [3,4] and, in Sec. 6, we give the summary and conclusions.

2 Applicability of first order perturbation to low-$E_\perp$ GIFAD

The first point we would like to address is the applicability of the classical FOP model to our work[3,4]. In this model, the *apparent* (a.k.a. *effective*) corrugation is proportional to the tangent of the rainbow angle. Based on this, the authors state that "any energy dependence in the SIVR corrugation of Bocan *et al.* [4], or equivalently η_a, will be manifested in the energy dependence of the rainbow angle and viceversa" (Eq. (3.39) and text following it, also repeated in the abstract and conclusions of Ref. [5]). However, low normal-energy GIFAD for He/KCl(001) is not within the range of validity of the FOP approach, as we can straightforwardly prove.

From our experimental and theoretical results for incidence respectively along the $\langle 110 \rangle$ (Figs. 2(a) and 3(a) of Ref. [3]) and $\langle 100 \rangle$ (Figs. 10 and 11 of Ref. [4]) channels, we show in Fig. 1 that, at low normal energies, the ratio of the tangent of the rainbow angle and the corrugation, $\tan(\Theta_{rb})/\Delta Z$, markedly de-

* Corresponding authors: gisela.bocan@cab.cnea.gov.ar, msilvia@iafe.uba.ar
[a] Address, Instituto de Nanociencia y Nanotecnología - Nodo Bariloche (CNEA-CONICET), Centro Atómico Bariloche, Av. Bustillo 9500, 8400 S.C. de Bariloche, Argentina.
[b] Address, Université Paris-Saclay, CNRS, Institut des Sciences Moléculaires d'Orsay, 91405, Orsay, France.
[c] Address, Université Paris-Saclay, CNRS, Institut des Sciences Moléculaires d'Orsay, 91405, Orsay, France.
[d] Address, Instituto Balseiro (U. N. Cuyo), Centro Atómico Bariloche, Av. Bustillo 9500, 8400 S.C. de Bariloche, Argentina.
[e] Address, Instituto de Astronomía y Física del Espacio (UBA-CONICET), C1428EGA Buenos Aires, Argentina.

parts from an $E_\perp$-independent behavior. This deviation from the FOP prediction is observed for both the intrinsic and apparent values of the involved quantities, where the former are derived solely from the equipotential curves of the theoretical potential energy surface (PES, obtained with the Perdew-Burke-Ernzenhof (PBE) [6] exchange-correlation functional), while the latter correspond to values obtained either from experiments or theoretical simulations which combine the mentioned PES (based on density functional theory calculations) with the surface initial-value representation (SIVR) approach.

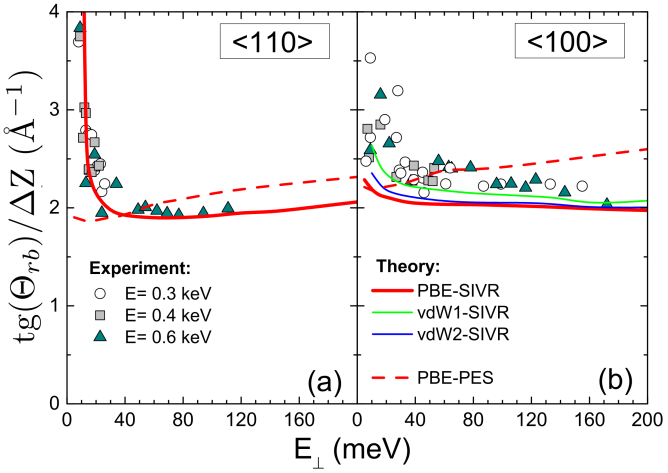

Fig. 1 Ratio $\tan(\Theta_{rb})/\Delta Z$ as a function of $E_\perp$ for He/KCl(001) GIFAD [3,4]. Note that b) includes two additional curves where the PBE exchange-correlation functional in the PES was modified to incorporate van der Waals (vdW) interactions [3,4].

Moreover, it is worth mentioning that our analysis of low-$E_\perp$ GIFAD for He-KCl(001) [3,4] shows that the PES regions affecting the corrugation are different from those relevant for the rainbow angle. That is, these two quantities probe different regions of the PES and hence do not provide the same information.

In addition, note that, following Eq. (3.30) in Ref. [5], the authors state that "For a hard wall potential, η_a is independent of the energy.". However, within a hard corrugated wall (HCW) model, the quantity η_a [Eq. (3.30)] gives the intrinsic corrugation, a quantity which is not $E_\perp$-independent, as it is respectively shown in Fig. 2 (a) of Ref. [3] and in Fig. 5 of Ref. [4] for the $\langle 110\rangle$ and $\langle 100\rangle$ channels.

3 Performance of a Morse-like potential for describing GIFAD of He-KCl(001)

In Secs. 2 and 4 of Ref. [5], the authors make use of a Morse-like potential to describe the atom-surface interaction in GIFAD. This is the second point we reckon as interesting for further looking into.

We here aim to verify i) to what extent the Morse formula, with a set of optimized parameters, can reproduce the DFT axial potential and ii) how the rainbow angle obtained when SIVR is combined with such Morse formula (instead of with the DFT potential) compares with both the experiments and the results from Fig. 2 of Ref. [5].

In the following study we disregard the FOP approximation of the Morse potential and consider instead the full formula from Eq. (2.3) [5], which we re-write as

$$V_M(y,z) = V_0\left[e^{-2\alpha(z-z_0-h_r h(y))} - 2e^{-\alpha(z-z_0-h_a h(y))}\right], \qquad (1)$$

where y is the coordinate across the incidence channel, z is the coordinate normal to the surface plane ($z=0$), and the function $h(y)$, defined as

$$h(y) = \cos\left(2\pi\frac{y}{D}\right), \qquad (2)$$

with D being the channel width [7], causes the position z of the physisorption well bottom to depend on y. In Eq. (1), z_0 is introduced to position the physisorption region outside the surface ($z>0$), V_0 is the well depth for the $h(y)=0$ case (for which the well bottom is located at $z=z_0$), α is a scaling factor (Allison *et al.* associate it with the potential softness), and the condition $h_r \neq h_a$ results in a well depth dependence on y. Note that z_0, V_0, α, h_r and h_a are parameters to be determined.

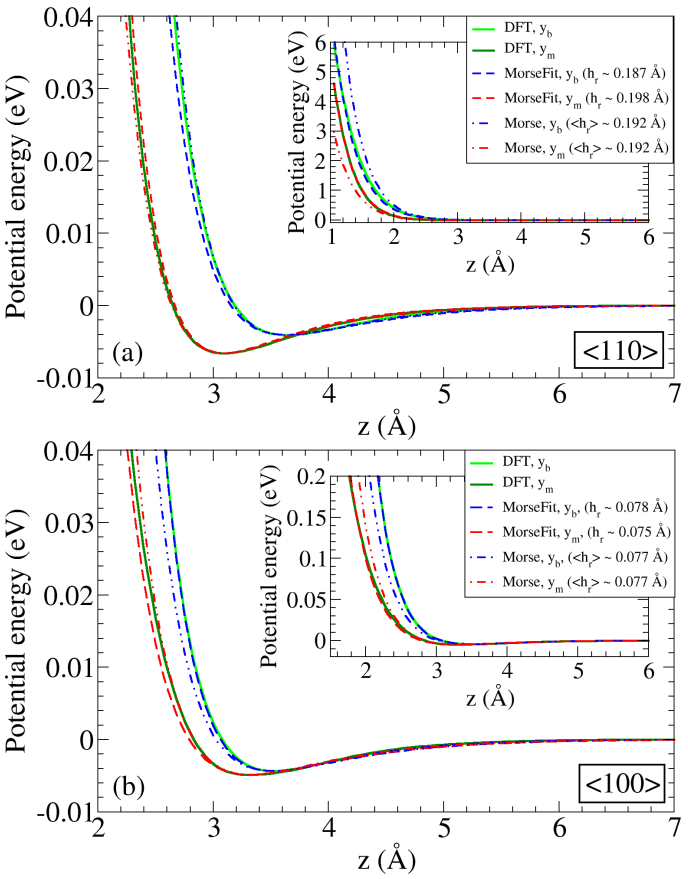

Fig. 2 DFT axial PES as a function of the He-surface distance z, for positions y_b (border) and y_m (middle), across the (a) $\langle 110\rangle$ and (b) $\langle 100\rangle$ channels. Also depicted, Morse fitting of these curves (dashed lines) and Morse potential for the average $\langle h_r\rangle$ (dashed-dot-dot lines). For $\langle 100\rangle$, the fitting was restricted to potential energies $V < 0.2$ eV, as explained in the text.

In Fig. 2 we show the DFT axial potential curves along $y=0$ (border of the channel, henceforth y_b) and $y=D/2$ (middle of the channel, henceforth y_m) for $\langle 100\rangle$ and $\langle 110\rangle$ channels. For

each incidence direction, we want the Morse potential $V_M(y,z)$ in Eq. (1) to best reproduce the corresponding DFT curves [3,4], with the focus on the features relevant for our reported low-$E_\perp$ GIFAD study. Hence, for each channel, we require $V_M(y_b,z)$ and $V_M(y_m,z)$ to match the corresponding DFT axial PESs at the bottom of the physisorption well. The positions and potential values extracted from the DFT axial PES, respectively labeled (z_b,V_b) and (z_m,V_m), are given in Table 1.

Table 1 From the DFT potential [3,4], position z and potential value V for the bottom of the physisorption well. For j=b,m, (z_j,V_j) corresponds to the y_j curve. Also, resulting values of the parameters z_0 and V_0 (from Eq. 3)

	channel $\langle 110\rangle$	channel $\langle 100\rangle$
z_b (Å)	3.637	3.516
V_b (eV)	-0.00406328	-0.00434379
z_m (Å)	3.093	3.322
V_m (eV)	-0.00659852	-0.00487556
z_0 (Å)	3.365	3.419
V_0 (Å)	0.00517799	0.00460200

Introducing this information into Eq. (1) for the y_b and y_m curves, we find

$$z_0 = \frac{z_m + z_b}{2}, \qquad V_0 = \sqrt{V_m V_b}. \tag{3}$$

Also, we are able to express the parameters h_a and α in terms of h_r as

$$\begin{aligned} h_a &= (z_m - z_b + 4h_r)/2, \\ \alpha &= [2(z_b - z_m - 2h_r)]^{-1} \ln\left(\frac{V_b}{V_m}\right), \end{aligned} \tag{4}$$

and hence $V_M(y_b,z)$ and $V_M(y_m,z)$ can be written in terms of a single parameter h_r as follows:

$$\begin{aligned} V_M(y_b,z) &= -V_b\left[(A_{h_r})^{2(z-z_b)} - 2\,(A_{h_r})^{z-z_b}\right], \\ V_M(y_m,z) &= -V_m\left[(A_{h_r})^{2(z-z_m)} - 2\,(A_{h_r})^{z-z_m}\right], \end{aligned} \tag{5}$$

where

$$A_{h_r} = \left(\frac{V_b}{V_m}\right)^{\frac{1}{2}\frac{1}{z_b - z_m - 2h_r}}.$$

The optimized value of h_r for a given channel could in principle be obtained from fitting either the y_b or the y_m DFT curve with the corresponding formula in Eq. (5), as illustrated in Fig. 2. However, we do encounter several difficulties upon attempting such fitting procedure. The first issue is that, for both channels, the resulting h_r varies within 5%, depending on which DFT curve we choose. This difference cannot be overlooked, given the high sensitivity of the Morse curve to the h_r value. The second issue is that the y_m curve for the $\langle 100\rangle$ channel is not satisfactorily fitted in the region of interest (low potential energy) unless we restrict the potential energy region to $V < 200$ meV, a problem likely related to the absence of surface atoms below $\langle 100\rangle$-midchannel. In order to pursue the Morse-DFT comparison, we use an average value of h_r. This works reasonably well for $\langle 110\rangle$ in the low-energy range but not much so for $\langle 100\rangle$, where the average h_r yields a sensitively lowered accord with the DFT potential, as shown in Fig. 2. These average values, depicted in Tab. 2, contradict Allison *et al.*'s claim (Ref. [5], Sec. 2, last paragraph) "The subtle variations in well depth calculated for example in [4], are reasonably well reproduced by choosing $h_a/h_r \approx 1$". Note that, for $\langle 100\rangle$, we get $h_a/h_r \simeq 0.73$, while for $\langle 110\rangle$, $h_a/h_r \simeq 0.59$.

Table 2 Averaged h_r parameter, from the border and midchannel fittings. Also, resulting values of h_a and α (Eq. (4). For the $\langle 100\rangle$ channel, fitting restricted to $V < 200$ meV for improved accord with the DFT potential in the region of interest

	channel $\langle 110\rangle$	channel $\langle 100\rangle$
h_r (Å)	0.192490	0.076570
h_a (Å)	0.112980	0.056140
α (1/Å)	1.524508	1.413209

For further visualization of the Morse formula performance, in Fig. 3 we compare, for both channels, the DFT equipotential curves with those obtained for the Morse potential, with the average h_r values given in Table 2.

The equipotential contours contain the $V(y_b,z)$ and $V(y_m,z)$ curves depicted in Fig. 2, but explore in addition how the potential energy behaves for intermediate positions $y_b < y < y_m$ across the channel. The main features in Figure 3 are that: a) For $\langle 110\rangle$ equpotentials, a simple trigonometric function, as given by Eq. (2) (following Allison *et al.* [5]), cannot account for the local maxima at mid-channel in the $V > 60$ meV DFT curves of the $\langle 110\rangle$ channel and, b) for $\langle 100\rangle$ equipotentials, the amplitudes (a.k.a. *intrinsic* corrugations) of the Morse curves are markedly smaller than the DFT ones. This expected difference is traced back to the already discussed difficulty of Eq. (1) to describe $V(y_m,z)$ for $\langle 100\rangle$, combined with the need of an averaged h_r (see Fig. 2 (b)). Note also that the amplitudes of Morse equipotential curves drive the maximum slopes (a.k.a. HCW rainbow angles), which also yield values much smaller than the ones obtained from DFT.

The next step is to analyze, for both channels, the extent to which the discussed differences between Morse and DFT potentials affect both the HCW and SIVR rainbow angles and how Morse-based calculations compare with our experiments from Refs. [3,4]. The rainbow angles derived for each of the cases just mentioned are depicted in Fig. 4. For $\langle 110\rangle$ (Fig. 4 (a)) Morse-based calculations give a reasonable accord with DFT-based ones (and hence, with experiments), despite the differences discussed between their respective equipotentials. The situation is very different for $\langle 100\rangle$ (Fig. 4 (b)). As we had anticipated when discussing the equipotential curves (Fig. 3 (b)), the HCW rainbow angles obtained from the Morse potential fall well below the DFT ones, and fail to follow their trend. These observations also apply to SIVR rainbow angles, and consequently lead Morse-SIVR results for $\langle 100\rangle$ to markedly underestimate the rainbow angles

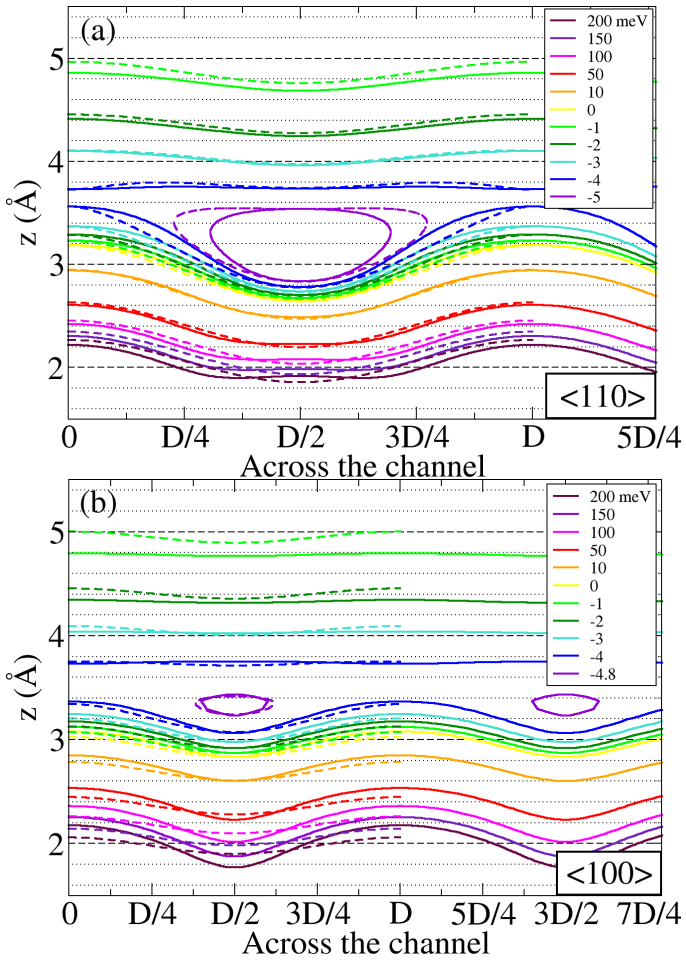

Fig. 3 Equipotentials for He-KCl(001) in 1-1 scale. DFT-PBE (solid lines), Morse formula (Eq. (1)), with the parameters from Tabs. 1 and 2 (dashed lines, plotted across a single channel). The channel widths are $D = 4.51229$ Å for $\langle 110 \rangle$ and $D = 3.19067$ Å for $\langle 100 \rangle$.

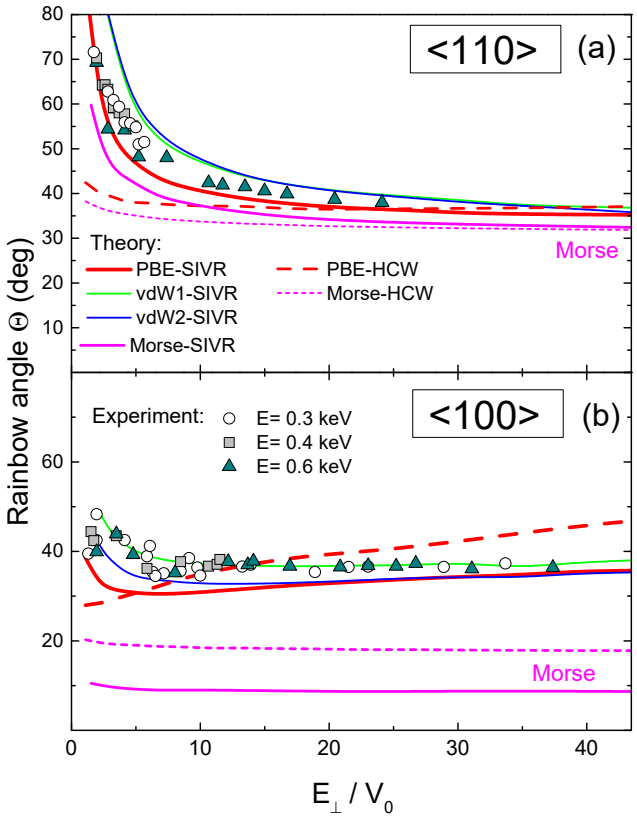

Fig. 4 Comparison of DFT and Morse rainbow angles as functions of $E_\perp/V_0$ for the incidence channel (a) $\langle 110 \rangle$ and (b) $\langle 100 \rangle$. Solid lines: DFT-SIVR (PBE, vdW1, vdW2) and Morse-SIVR results; dashed lines: HCW-PBE and HCW-Morse values. The Morse potential was obtained with the average h_r value given in Tab. 2.

derived from the experiments. Particularly, note that the Morse-SIVR approach fails to capture the magnitude of the rainbow angle increase with decreasing very low $E_\perp$. At this point, it is enlightening to discuss Fig. 2 of Ref.[5] and how it relates to our Fig. 4 (b), this latter plotted in terms of $E_\perp/V_0$ to facilitate this comparison. From the caption of Allison's Fig. 2, we understand that the considered channel is $\langle 100 \rangle$. In Allison's FOP model, and considering $h_r \simeq h_a$, the rainbow angle is given by the parameter K_{hw} (Sec. 3.4 in Ref. [5]), which is set to 35° in order to match our PBE-SIVR value for the $E_\perp/V_0 > 20$ region. From their Eq. (3.21), which reads $K_{hw} = 2\pi h_r/D$ (adapted to our notation, D is the channel width for $\langle 100 \rangle$), they obtain $h_r \approx 0.3102$ Å, a value that markedly differs from our optimized $h_r = 0.07657$ Å. Hence, in Fig. 2 of Ref. [5], the authors show that an increasing behavior of the rainbow angle for decreasing low $E_\perp$ is obtained from their Morse-like formula, within the FOP model and for the condition $h_a/h_r < 1$, but they do not provide a realistic He-KCl(001) potential.

4 About experimental processing of GIFAD patterns

The third point deals with the need to clarify some concepts and procedures in our work [3,4] that were questioned by Allison *et al.*

We agree with Allison *et al.* on the need to differentiate the *intrinsic* corrugation, obtained from the interaction potential, from the *apparent* one, which is influenced by dynamic effects. Allison *et al.* in Ref. [5] deem our comparing both quantities in a figure "unhelpful", while we consider it provides a visualization of the relevance of dynamic effects in the *apparent* corrugation. We never refer to the latter as "dynamic corrugation" (a somewhat misleading expression), as the authors wrongly claim [in the Abstract, and also in Secs. 2, 3.5, and 5].

The procedure used to obtain the rainbow angle and the corrugation from the experimental patterns, judged as "not very illuminating" [Sec. 5 of Ref. [5]], is based on the idea of an equivalent HCW system [2,3,8]; that is, on the determination of an equipotential curve which yields the experimental intensity profile within a HCW model. This procedure by no means implies that the determined equipotential curve corresponds to the potential of the real, non HCW, system.

Regarding the rainbow angle and the authors' statement about

it being ill-defined in quantum mechanics [Sec. 3.2 in Ref. [5]], we agree that within an ideal mathematical treatment, a grazing, monoenergetic, fully collimated, atomic beam that ellastically diffracts from a crystalline surface might yield no rainbow peaks, given the likely null overlapping between the intrachannel rainbow maximum and the almost Dirac-delta shape of the nearest (interchannel) Bragg peak. However, in a realistic non-ideal experiment, as well as in our semi-quantum model, the beam is not mathematically collimated and hence a non-zero rainbow-Bragg overlapping may occur.

5 Unexpectedness of our results

Finally, in Sec. 1 of Ref. [5], the authors question the unexpectedness of our results of Ref. [3], based on Refs. [9–11]. We thank the authors for bringing these works up to our attention. In fact, we believe the rainbow behavior experimentally observed in Refs. [10,11] is an interesting antecedent to the low-$E_\perp$ features in both the corrugation and the rainbow, reported in GIFAD [3,4,12–14]. In relation to the theoretical article by Pollak and Miret-Artés [9], we did not find any mention to the increase of the rainbow angle with decreasing energy, but this behavior was explicitly discussed in a previous article by the same authors[15]. However, we must stress that these articles [9,11,15] address Ar-LiF(001) scattering in non-GIFAD conditions and that, while Kondo *et al*. find this feature "counterintuitive" [11], Miret-Artés and Pollak argue against a decreasing corrugation (for increasing $E_\perp$ in the low $E_\perp$ region) in the following terms: "The decrease of the rainbow angles with energy is the result of dynamics and does not imply that the corrugation becomes smaller with increasing energy as suggested by Kondo *et al*." [Ref. [15], p. 180]. In this context, our report of an impressive $\gtrsim 85\%$ corrugation increase (for decreasing $E_\perp$ in the low $E_\perp$ region, relative to the 100 meV value), markedly sharper and larger than those previously observed (though not thoroughly discussed) in GIFAD for similar systems [12,13] well deserves to be described as "unexpected". Remarkably, this corrugation feature cannot be fully explained in terms of dynamic effects. The increasing intrinsic corrugation (with decreasing $E_\perp$) is a key factor of the observed behavior.

6 Summary and conclusions

In Summary, in this comment we have analyzed the applicability of Allison *et al*.'s FOP model and Morse-like potential for describing GIFAD as reported in our articles[3,4] for a realistic He-KCl(001) system. In addition, we answer some specific remarks made by the authors regarding those articles. We thank Allison *et al*. for their interesting and motivating work which gave us the opportunity to revisit our own and clarify some concepts and explanations. Interaction and exchange of ideas is always enriching. Their qualitative discussion does not debunk or contradict any of our conclusions.

Author Contributions

All the authors were involved in the discussion and analysis reported in this comment as well as in the editing and reviewing of the manuscript. The original draft was written by G. A. Bocan and M. S. Gravielle.

Conflicts of interest

There are no conflicts of interest to declare.

Acknowledgements

The authors acknowledge financial support of ANPCyT (PICT-2017-1201, PICT-2017-2945, PICT-2020-1755 and PICT-2020-1434), CONICET (PIP 112 201301 00386 CO and PIP 112 202101 00411 CO), and U. N. Cuyo (06/C025-T1).

Notes and references

1 H. Winter and A. Schüller, *Prog. Surf. Sci.*, 2011, **86**, 169–221.
2 H. Khemliche, P. Rousseau, P. Roncin, V. H. Etgens and F. Finocchi, *Appl. Phys. Lett.*, 2009, **95**, 151901.
3 G. A. Bocan, H. Breiss, S. Szilasi, A. Momeni, M. E. Staicu Casagrande, M. S. Gravielle, E. A. Sánchez and H. Khemliche, *Phys. Rev. Lett*, 2020, **125**, 096101.
4 G. A. Bocan, H. Breiss, S. Szilasi, A. Momeni, M. E. Staicu Casagrande, E. A. Sánchez, M. S. Gravielle and H. Khemliche, *Phys. Rev. B*, 2021, **104**, 235401.
5 W. Allison, S. Miret-Artés and E. Pollak, *Phys. Chem. Chem. Phys.*, 2022, **24**, 15851–15859.
6 J. P. Perdew, K. Burke and M. Ernzerhof, *Phys. Rev. Lett.*, 1996, **77**, 3865–3868.
7 We have redefined $h(y)$ so that its maximum at the border of the channel and minimum at midchannel respectively correspond to $y = 0$ and $y = D/2$.
8 M. Debiossac, P. Pan and P. Roncin, *Phys. Chem. Chem. Phys.*, 2021, **23**, 7615–7636.
9 E. Pollak and S. Miret-Artés, *J. Phys. Chem. C*, 2015, **119**, 14532–14541.
10 E. Schweizer, C. Rettner and S. Holloway, *Surf. Sci.*, 1991, **249**, 335–349.
11 T. Kondo, H. S. Kato, T. Yamada, S. Yamamoto and M. Kawai, *Eur. Phys. J. D*, 2006, **38**, 129–138.
12 A. Momeni, P. Soulisse, P. Rousseau, H. Khemliche and P. Roncin, *e-J. Surf. Sci. Nanotech.*, 2010, **8**, 101–104.
13 P. Soulisse, *PhD thesis https://tel.archives-ouvertes.fr/tel-00625450/ Orsay*, 2011, 1–211.
14 U. Specht, M. Busch, J. Seifert, H. Winter, K. Gärtner, R. Włodarczyk, M. Sierka and J. Sauer, *Nucl. Instrum. Meth. Phys. Res. B*, 2011, **269**, 799–803.
15 S. Miret-Artés and E. Pollak, *Surf. Sci. Rep.*, 2012, **67**, 161–200.